A novel metal-organic framework based on hexanuclear Co(II) clusters: structure, magnetism and its application as an anode material for lithium-ion battery

Yuan-Chun He,*[a] Yang Yu,[a] Lingyan Wang,[a] Jiaqin Yang,[a] Wei-Qiu Kan,*[b] Yan Yang,[c] Yao-Yao Fan,[a] Zhihong Jing,[a] Jinmao You*[ad]

[a] *College of Chemistry and Chemical Engineering, Qufu Normal University, Qufu 273165, P. R. China*

[b] *Jiangsu Province Key Laboratory for Chemistry of Low-Dimensional Materials, School of Chemistry and Chemical Engineering, Huaiyin Normal University, Huaian 223300, P. R. China*

[c] *School of Material Science and Chemical Engineering, Xi'an Technological University, Xi'an 710021 P. R. China*

[d] *Key Laboratory of Tibetan Medicine Research, Northwest Institute of Plateau Biology, Chinese Academy of Science, Xining, P. R. China*

Physical measurements

PXRD patterns were conducted on a Rigaku Dmax 2000 X-ray diffractometer with graphite monochromatized Cu K_α radiation (λ = 0.154 nm) at 2θ ranging from 5 to 50°. The C, H and N elemental analyses were measured on a Perkin–Elmer 2400 elemental analyzer. Infrared (IR) spectra were carried out on a Mattson Alpha-Centauri spectrometer at the range of 4000–400 cm^{-1}. Thermogravimetric analyses were performed on a Perkin-Elmer TG-7 analyzer heated from room temperature to 600 °C under nitrogen. The scanning electron microscopy (SEM) images were taken by using a JEOL-JSM-6700F field-emitting (FE) scanning electron microscope. X-ray photoelectron spectroscopy (XPS) was recorded on a PHI quantera SXM spectrometer with an Al Kα = 280.00 eV excitation source. Variable-temperature magnetic susceptibility data were obtained using a SQUID magnetometer (Quantum Design, MPMS-5) with an applied field of 1000 Oe in the temperature range of 2-300 K. Transmission electron microscopy (TEM) images were acquired on a JEM-2100 electron microscope operated at 200 kV.

Electrochemical measurements

Compound **1** and Co_3O_4@C were ground into powder and used as the active materials, respectively. The active materials (60 wt%), acetylene black (30 wt%) and poly (vinylidenefluoride) (PVDF) (10 wt%) with *N*-methyl-2-pyrrolidone (NMP) were mixed carefully to form a homogeneous slurry, which was coated on a copper foil and dried at 100 °C for 12 h in vacuum. The mass loading of active material in the electrode was around 1.5 mg cm^{-2}, and the thickness of the electrode is around 20 μm. In an argon-filled glovebox, the cathode and anode (lithium foil) were separated by celgard 2400 as the separator with a solution of 1.0 M $LiPF_6$ in ethylene carbonate (EC)/diethyl carbonate (DEC) (1:1 by volume) as the electrolyte, and the coin cells were assembled successfully. The galvanostatic charge and discharge tests were carried out on a Land automatic battery tester (Wuhan, China) at 298 K.

X-ray crystallography

Single-crystal X-ray diffraction data for **1**were recorded on an Oxford Gemini R Ultra diffractometer with graphite-monochromated Mo-Kα radiation (λ = 0.71073 Å) at 293 K. All the structures were solved by Direct Method of SHELXS-97 and refined by full-matrix least- squares techniques using the SHELXL-97 program within WINGX.[1] Non-hydrogen atoms were refined anisotropically, and hydrogen atoms of ligands were located at their calculated positions. Selected bond distances and angles for **1** are given in Table S2.

Magnetic Properties

The temperature-dependent magnetic susceptibility was measured on powder sample of compound **1** at 1000 Oe in the range of 2-300 K. The $\chi_m T$ and $1/\chi_m$ versus T plots are shown in Fig. S9. The $\chi_m T$ value of [Co_6] cluster at 300 K is 21.2 cm^3 mol^{-1} K, which is larger than the value six magnetically isolated spin-only S = 3/2 Co^{2+} systems (11.3 cm^3 mol^{-1} K). It reveals the significant orbit contribution to high-spin Co^{2+} cation in an octahedral coordination environment. As temperature decreases, the $\chi_m T$ value decreases smoothly to reach a minimum value of 14.5 cm^3 mol^{-1} K at 20 K, then increases rapidly to 16.7 cm^3 mol^{-1} K at 2 K. Above 50 K, the temperature dependence of $1/\chi_m$ obeys the Curie-Weiss law with C = 25.0 cm^3 mol^{-1} K and θ = -29.0 K, which suggests dominant antiferromagnetic interactions between the [Co_6] cluster and the presence of spin-orbit couplings.

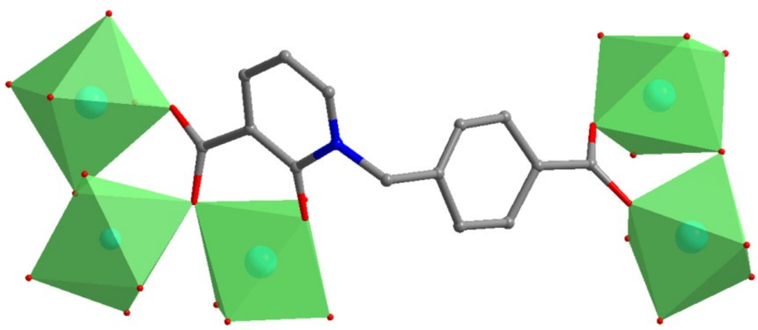

Fig. S1 Coordination mode of organic ligand.

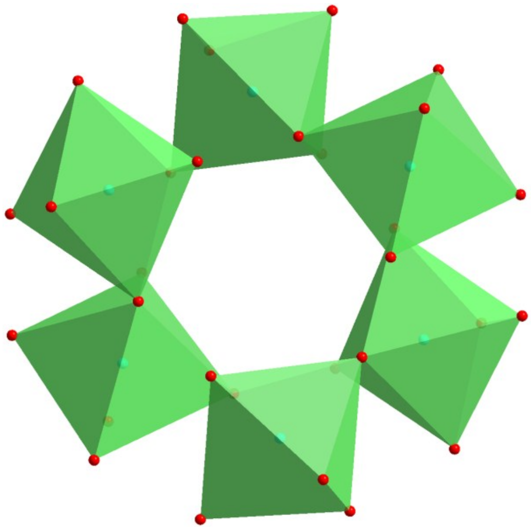

Fig. S2 View of the hexanuclear [Co_6] cluster.

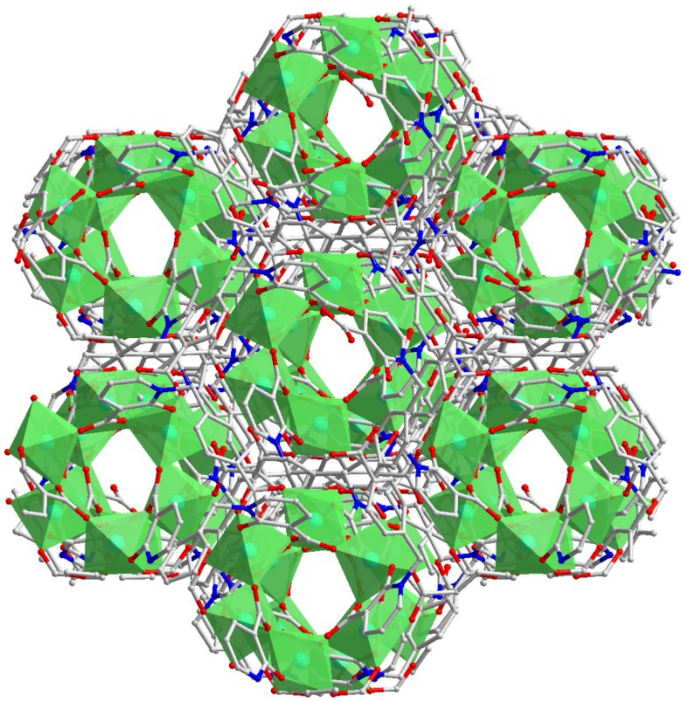

Fig. S3 View of the 3D framework.

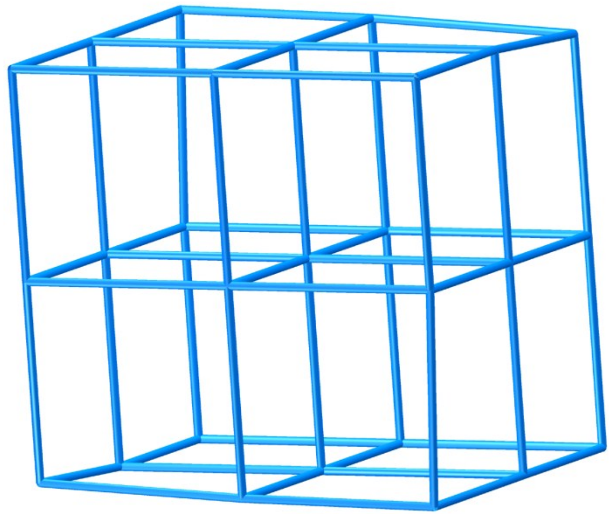

Fig. S4 View of the 6-connected net with Schläfli symbol of $4^{12}\cdot6^{3}$.

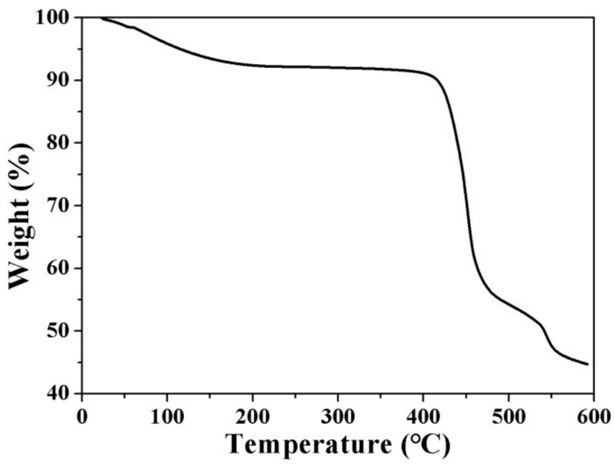

Fig. S5 TG curve of compound **1**.

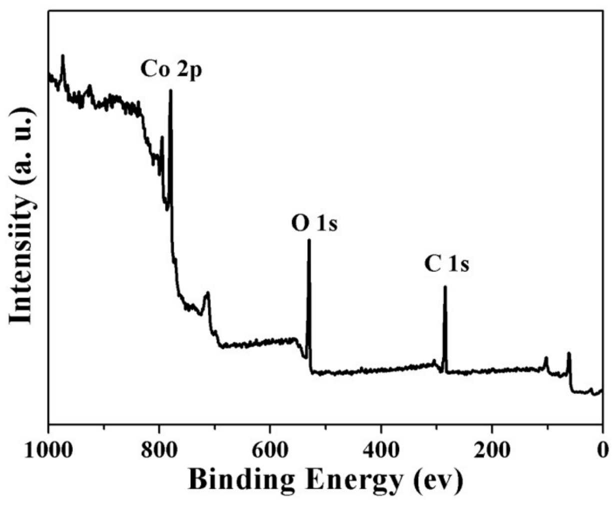

Fig. S6 XPS spectrum of Co_3O_4@C.

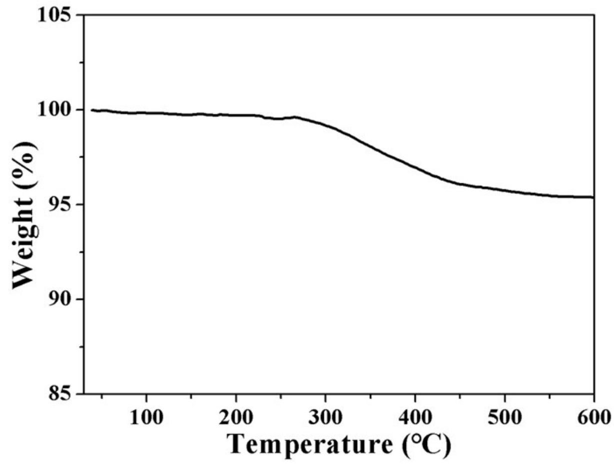

Fig. S7 TG curve of Co_3O_4@C.

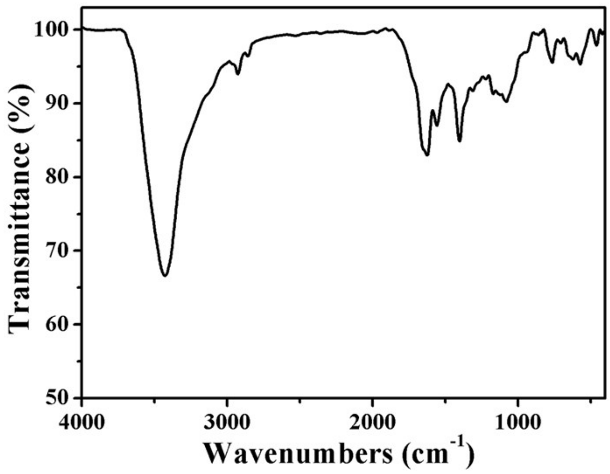

Fig. S8 IR spectrum of compound **1**.

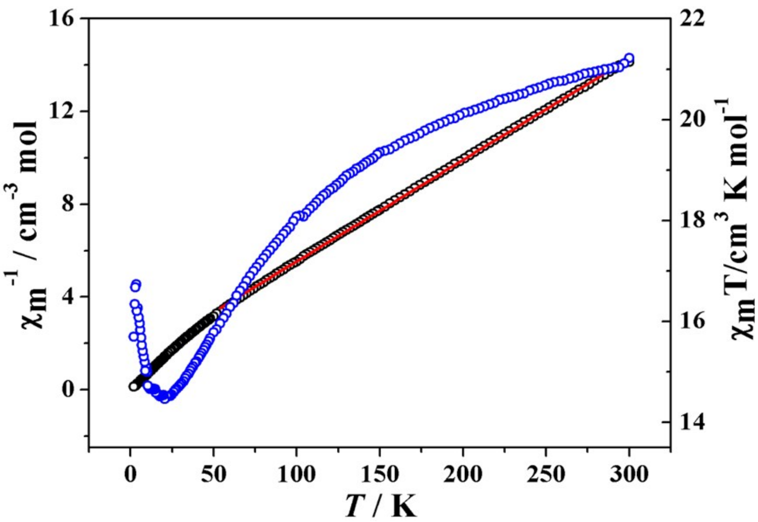

Fig. S9 Temperature dependence of $\chi_m T$ and $1/\chi_m$ versus T plots for compound **1**.

Table S1 Comparison of the electrochemical performaces of Co-MOFs derived materials reported in the literatures

Samples	Current density/mA g^{-1}	Cycles	Capacity/mA h g^{-1}	Reference
Co_3O_4@C	100	30	796	This work
	4000	1000	197	
Co_3O_4	500	50	574	2
	2000	50	569	
Co_3O_4@C	100	100	1137	3
Co_3O_4	100	100	762	4
Co_3O_4	100	80	683	5
Co_3O_4	100	200	787	6
Co_3O_4@C	89	200	877	7
Co_3O_4	100	100	886	8

Table S2 Selected bond distances (Å) and angles (°) for **1**.

Co(1)-O(4)$^{\#1}$	2.035(4)	Co(1)-O(5)$^{\#2}$	2.063(5)
Co(1)-O(1)$^{\#2}$	2.069(4)	Co(1)-O(1)	2.095(4)
Co(1)-O(3)$^{\#3}$	2.116(5)	Co(1)-O(2)$^{\#4}$	2.133(5)
O(4)$^{\#1}$-Co(1)-O(5)$^{\#2}$	90.5(2)	O(4)$^{\#1}$-Co(1)-O(1)$^{\#2}$	176.03(19)
O(5)$^{\#2}$-Co(1)-O(1)$^{\#2}$	85.72(17)	O(4)$^{\#1}$-Co(1)-O(1)	89.66(18)
O(5)$^{\#2}$-Co(1)-O(1)	178.08(19)	O(1)$^{\#2}$-Co(1)-O(1)	94.1(2)
O(4)$^{\#1}$-Co(1)-O(3)$^{\#3}$	87.95(19)	O(5)$^{\#2}$-Co(1)-O(3)$^{\#3}$	89.80(19)
O(1)$^{\#2}$-Co(1)-O(3)$^{\#3}$	93.18(17)	O(1)-Co(1)-O(3)$^{\#}$3	92.12(17)
O(4)$^{\#1}$-Co(1)-O(2)$^{\#4}$	88.44(19)	O(5)$^{\#2}$-Co(1)-O(2)$^{\#4}$	82.46(19)
O(1)$^{\#2}$-Co(1)-O(2)$^{\#4}$	89.92(18)	O(1)-Co(1)-O(2)$^{\#4}$	95.63(17)
O(3)$^{\#3}$-Co(1)-O(2)$^{\#4}$	171.43(18)		

Symmetry transformations used to generate equivalent atoms: $^{\#1}$ x+1/3,x-y-1/3,z+1/6; $^{\#2}$ x-y,x,-z; $^{\#3}$ y+2/3,x+1/3,-z-1/6; $^{\#4}$ y,-x+y,-z.

1 (a) G. M. Sheldrick, SHELXL-97, Programs for X-ray Crystal Structure Solution; University of Göttingen: Göttingen, Germany, 1997; (b) G. M. Sheldrick, SHELXL-97, Programs for X-ray Crystal Structure Refinement; University of Göttingen: Göttingen, Germany, 1997; (c) L. J. Farrugia, WINGX: A Windows Program for Crystal Structure Analysis; University of Glasgow: Glasgow, UK, 1988.

2 W.-W. Shi, H. Zhang, X.-Y. Zheng, S.-F. Lou, B.-W. Hu, G.-P. Yin and Y.-Z. Gao, *New J. Chem.*, 2017, **41**, 6187–6194.

3 B. Qiu, W. Guo, Z. Liang, W. Xia, S. Gao, Q. Wang, X. Yu, R. Zhao and R. Zou, *RSC Adv.*, 2017, **7**, 13340–13346.

4 F. Zhang, D.-D. Qi and X.-G. Zhang, *Int. J. Electrochem. Sci.*, 2016, **11**, 189–199.

5 J. Chen, X. Mu, M. Du and Y. Lou, *Inorg. Chem. Commun.*, 2017, **84**, 241–245.

6 Y. Chen, Y. Wang, H. Yang, H. Gan, X. Cai, X. Guo, B. Xu, M. Lü and A. Yuan, *Ceram. Int.*, 2017, **43**, 9945–9950.

7 G. Wang, F. Zhu, J. Xia, L. Wang, Y. Meng and Y. Zhang, *Electrochimica Acta*, 2017, **257**, 138–145.

8 F. Zheng, Z. Yin, H. Xia and Y. Zhang, *Mater. Lett.*, 2017, **197**, 188–191.